GEOPHYSICS, VOL. 57, NO. 8 (AUGUST 1992); P. 1004–1013, 10 FIGS., 2 TABLES.

Two-dimensional inversion filters in magnetic prospecting: Application to the exploration for buried antiquities

Gregory N. Tsokas* and Constantinos B. Papazachos*

ABSTRACT

The magnetic total field anomaly is considered as the convolution of two analytically determined functions. One of them is chosen such that it modifies the amplitude of the anomaly while the other controls the anomaly pattern. Using the anomaly of vertical-sided finite prisms, the inverse of the shape function is computed in the Wiener mode. This is an optimum filter operator, in the least-square sense, to be convolved with the data.

The majority of the structures which are the targets of exploration at archaeological sites can be represented as assemblages of vertical-sided prisms. This fact motivates the selection of the basic model. On that basis the filtering scheme results in anomalies centered at the epicenter of the disturbing bodies, delineates their lateral extent fairly well, and gives a measure of their magnetization.

Applications of synthetic and actual data clarify the merits and disadvantages of the technique.

INTRODUCTION

The aim of "archaeological geophysics" is to locate and identify buried ancient relics. However, archeologists are very often forced to decide upon expropriation of lands if antiquities are concealed there. Therefore, more information is required about subsurface conditions than simply pinpointing target locations beneath pronounced geophysical anomalies. The survey is considered to be successfully completed if it has as a final product a map that more or less gives the plan view of the concealed structures, i.e., the result that would have been drawn if an excavation had taken place (Scollar et al., 1986; Wynn 1986).

The present study comprises an effort to achieve the presentation of the total magnetic field maps over buried antiquities in an easily readable form. This form should give an outline of the dimensions of buried structures, present their centers at their actual locations (within the range of accuracy), and of course, be as reliable as possible.

The problem is solved by means of inverse filtering. The convolutional model of the total magnetic field anomaly is necessary for this procedure to be applicable. An analogous model was proposed in Bhattacharrya and Navolio (1975) and Bhattacharrya and Chan (1977).

Karousova and Karous (1989) proposed the exploitation of inverse filtering in the geophysical search for antiquities. They constructed the appropriate filters for a vertical cylinder and an infinite prism. Tsokas et al. (1991) attempted to modify the procedure described by the former researchers. They used filters that employed the anomaly caused by a finite prism model and convolved each profile of the geophysical map with these. In this way, the most commonly applicable model was used in a pseudo-two-dimensional procedure. Additionally, they commented on the filter's truncation length.

The present study is aimed toward a fully two-dimensional (2-D) procedure. Such a procedure should be relatively simple and easily applicable to meet the requirements of swift application even "in situ."

THE CONVOLUTIONAL MODEL

McGrath and Hood (1973) proposed an algorithm for the magnetic effect over any prism-shaped body. The geometrical models are generated by the addition of thin plates, and the net effect is computed by numerical integration of the respective thin-plate effects. According to that algorithm, the following equation (Grant and West, 1965; McGrath and Hood, 1973) gives the magnetic effect over a thin plate:

$$\Delta T(x, y) = J \cdot s \cdot b \cdot c \cdot [f(x, y + Y) - f(x, y - Y)], \quad (1)$$

where

$$f(x, y + Y) = T_1 - T_2 - T_3 \cdot (T_4 + T_5) - T_6 \cdot T_7. \quad (2)$$

Manuscript received by the Editor May 31, 1991; revised manuscript received December 10, 1991.
*Geophysical Laboratory, Dept. of Geology, Aristotle University of Thessaloniki, Thessaloniki 540 06, Greece.

Figure 1 shows a dipping thin plate that strikes along the Y-axis of an orthogonal coordinate system. The symbols used and their meaning are listed below.

LIST OF SYMBOLS

J = intensity of magnetization
T = earth's total magnetic field intensity
s = thickness of the plate
$b = (\sin^2 i + \cos^2 i \sin^2 d)^{1/2} = \sin i/\sin \gamma$
$c = (\sin^2 I + \cos^2 I \sin^2 D)^{1/2} = \sin I/\sin \beta$
I = angle of inclination of the earth's magnetic field
i = angle of inclination of the magnetization (−180 to 180 degrees)
d = angle between the horizontal projection of J and the positive Y-axis
D = angle between the horizontal projection of T and the positive Y-axis
Y = half-strike length of the plate
$c^2 = (x - \ell \cos f)^2 + (h + \ell \sin f)^2$
θ = angle of dip of plate
ℓ = width of the plate
h = depth of the plate
$E^2 = x^2 + h^2$
$B = x \sin \theta + h \cos \theta$
$c = h \sin \theta - x \cos \theta$
β = angle of inclination of the component of T in the xz-plane,
$= \tan^{-1} (\tan I/\sin D)$,
γ = angle of inclination of the component of J in the xz-plane,
$= \tan^{-1} (\tan i/\sin d)$.

The quantities on the right-hand side of equation (2) are defined as follows:

$$T_1 = \left[\frac{y + Y}{(c^2 + (y + Y)^2)^{1/2}}\right] \cdot \left[\frac{(x - \ell \cdot \cos\theta) \cdot \cos\alpha - (h + \ell \cdot \sin\theta) \cdot \sin\alpha}{c^2}\right],$$

$$T_2 = \frac{y + Y}{(E^2 + (y + Y)^2)^{1/2}} \cdot \left[\frac{x \cdot \cos\alpha - h \cdot \sin\alpha}{E^2}\right],$$

$$T_3 = \frac{1}{B^2 + (y + Y)^2} \cdot \left[\frac{A + \ell}{[c^2 + (y + Y)^2]^{1/2}} - \frac{A}{[E^2 + (y - Y)^2]^{1/2}}\right],$$

$$T_4 = (\cos\alpha \cdot \cos\theta - \cos\beta \cdot \cos\gamma + \cos\beta \cdot \cot D \cdot \cos\gamma \cdot \cot d) \cdot (y + Y),$$

$$T_5 = (\cos\gamma \cdot \cot d \cdot \sin(\theta - \beta) + \cos\beta \cdot \cot D \cdot \sin(\theta - \gamma)) \cdot B,$$

$$T_6 = \cos\gamma \cdot \cot d \cdot \cos(\theta - \beta) + \cos\beta \cdot \cot D \cdot \cos(\theta - \gamma),$$

$$T_7 = \frac{1}{[c^2 + (y + Y)^2]^{1/2}} - \frac{1}{[E^2 + (y + Y)^2]^{1/2}},$$

where $\alpha = \beta + \gamma - \theta$.

We now consider a model that resembles the majority of structures occurring in archaeological search: a rectangular vertical-sided prism. This choice is well justified since the most commonly met features can be represented as a series of such "blocks." For instance, the concealed features are usually building foundation relics, roads, tombs, defense wall relics, ditches, etc.

Consequently, following the initial algorithm, we consider the vertical-sided rectangular prism of Figure 2 as being represented by a series of thin plates. Because of the superposition principle, the magnetic effect that the prism

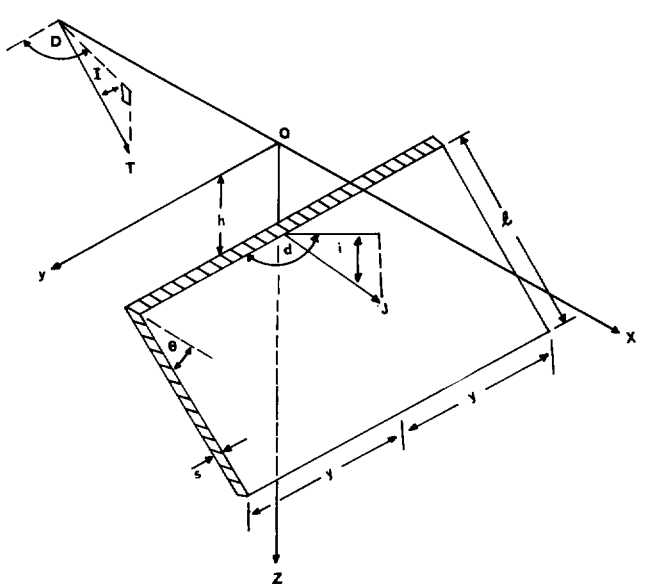

FIG. 1. View of the thin plate model (from McGrath and Hood, 1973).

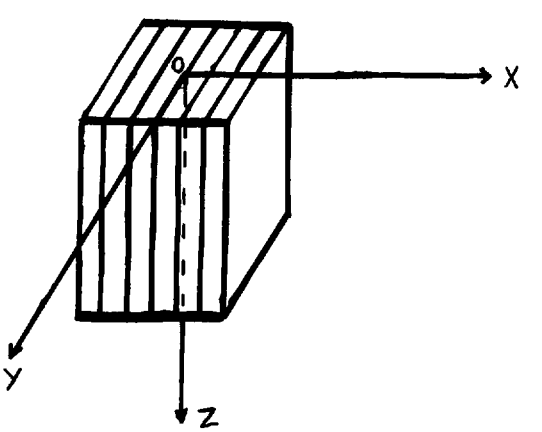

FIG. 2. View of the vertical-sided prism composed of a number of thin plates.

produces can be calculated as the sum of the effects of the individual thin plates. This is given by the following equation:

$$\Delta T(x,y) = J \cdot s \cdot b \cdot c \sum_{i=1}^{N} [f_i(x,y+Y) - f_i(x,y-Y)], \quad (3)$$

where N is the number of thin plates that represent the prism.

Equation (3) can be written as the product of two functions, say D and R. If we define

$$D = J \quad (4)$$

then this factor can be reasonably termed the "amplitude function" because it modulates the strength of the anomaly. The function

$$R(x, y) = s \cdot b \cdot c \cdot \sum_{i=1}^{N} [f_i(x, y+Y) - f_i(x, y-Y)] \quad (5)$$

can be termed the "shape function" since it controls the shape of the anomaly. Hence, equation (3) can be represented as

$$\Delta T(x, y) = D \cdot R(x, y) \quad (6)$$

To proceed in a convolutional model the following assumptions must hold:

1) The magnetization of the thin plates is of the induced type or, at least, is along a known direction.
2) Any structure or irregular shape can be simulated by an assemblage of elementary bodies of simple geometrical shape. These pieces should be similar in shape and buried at equal depths.

The validity of the above assumptions is not at the expense of generality. Induced magnetization can be considered as basically responsible for the anomalies over buried relics, except for special situations (such as buried kilns) where there is no need for any sort of filtering. On the other hand, the second assumption is self evident in archaeological geophysics.

Consider an ensemble of bodies similar to the one given in Figure 2, placed at the same depth at points (x, y) given by

$$x_\ell = \ell \Delta x \qquad \ell = L_1, \ldots, L_2$$

$$y_m = m \Delta y \qquad m = M_1, \ldots, M_2,$$

where Δx and Δy are the digitization intervals along the x- and y-axis, respectively. For the sake of simplicity, we can assume that Δx is equal to Δy.

By the superposition principle, the total field anomaly that the bodies produce can be written as:

$$\Delta T(x_i, y_j) = \sum_{\ell=L_1}^{L_2} \sum_{m=M_1}^{M_2} D_{\ell,m} \cdot R(x_i - x_\ell, y_j - y_m)$$

$$i = L_1, \ldots, L_2 \qquad j = M_1, \ldots, M_2. \quad (7)$$

Equation (7) is an expression of 2-D convolution which becomes more obvious if we rewrite it as:

$$T_{ij} = \sum_{\ell=L_1}^{L_2} \sum_{m=M_1}^{M_2} D_{\ell m} \cdot R_{i-\ell, j-m}, \quad (8)$$

where $\Delta T(x_i, y_j) = T_{ij}$ and $R(x_i - x_\ell, y_j - y_m) = R_{i-\ell' j-m}$. The same equation can now be represented in a simpler form as

$$\underline{\mathbf{T}} = \underline{\mathbf{D}} * \underline{\mathbf{R}}. \quad (9)$$

The spatial distribution of the amplitude function $\underline{\mathbf{D}}$ can be obtained from equation (9) by convolution with the inverse filter $\underline{\mathbf{R}}^{-1}$. Hence,

$$\underline{\mathbf{D}} = \underline{\mathbf{T}} * \underline{\mathbf{R}}^{-1} \quad (10)$$

given that $\underline{\mathbf{R}} * \underline{\mathbf{R}}^{-1} = \underline{\boldsymbol{\theta}}$, where $\underline{\boldsymbol{\theta}}$ is the unit element for deconvolution, that is, an infinite matrix with $\underline{\boldsymbol{\theta}}_{ij} = 0$ except for $\underline{\boldsymbol{\theta}}_{00}$ that is equal to 1.

The inversion of $\underline{\mathbf{R}}$ results in a filter infinitely extended in both directions. For the sake of simplicity, we prefer the truncated inverse filter denoted by $\bar{\underline{\mathbf{R}}}^{-1}$. The optimum inverse filter coefficients $\bar{R}_{ij}^{-1}$ are produced by the minimization of the sum of the square errors $E = \underline{\mathbf{R}} * \bar{\underline{\mathbf{R}}}^{-1} - \underline{\boldsymbol{\theta}}$.

Such a finite filter, which is optimum in a least-squares sense, is given by

$$\sum_{j=L_1}^{L_2} \sum_{i=M_1}^{M_2} R_{i,j}^{-1} \cdot A_{k-i,\ell-j} = R_{-k,-\ell}$$

$$k = M_1, \ldots, M_2 \qquad \ell = L_1, \ldots, L_2, \quad (11)$$

where $A_{k,\ell}$ is the autocorrelation of the shape function. Equation (11) is an extension to two dimensions of the spiking deconvolution equation (Kanasewitch, 1975).

APPLICATIONS HINTS

The system of equations (11) can also be written as:

$$\bar{\underline{\mathbf{R}}}^{-1} \cdot \underline{\mathbf{A}} = \underline{\mathbf{R}} \quad (12)$$

where $\bar{\underline{\mathbf{R}}}^{-1}$ and $\underline{\mathbf{R}}$ are 2-D $(M_2 - M_1 + 1) \times (L_2 - L_1 + 1)$ matrices and $\underline{\mathbf{A}}$ is a four-dimensional (4-D) $(M_2 - M_1 + 1) \times (L_2 - L_1 + 1) \times (M_2 - M_1 + 1) \times (L_2 - L_1 + 1)$ matrix, and where:

$$(\bar{\underline{\mathbf{R}}}^{-1})_{ij} = \bar{R}_{i,j}^{-1}, \ (\underline{\mathbf{R}})_{k\ell} = R_{-k,-\ell}$$

and

$$(\underline{\mathbf{A}})_{ijk\ell} = A_{k-i,\ell-j}.$$

Because the calculation of the inverse matrix of $\underline{\mathbf{A}}$ is complicated, we want to formulate equation (11) in a different way. We thus take the $(L_2 - L_1 + 1)$ columns of $\bar{\underline{\mathbf{R}}}^{-1}$ and $\underline{\mathbf{R}}$ and rearrange them to form two column vectors $\bar{\mathbf{R}}'^{-1}$ and $\mathbf{R}'$ as follows:

$$\bar{\mathbf{R}}'^{-1} = \begin{bmatrix} \bar{R}^{-1}_{M_1,L_1} \\ \bar{R}^{-1}_{(M_1+1),L_1} \\ \cdot \\ \cdot \\ \bar{R}^{-1}_{M_2,L_1} \\ \bar{R}^{-1}_{M_1,(L_1+1)} \\ \cdot \\ \cdot \\ \bar{R}^{-1}_{M_1,L_2} \\ \cdot \\ \cdot \\ \bar{R}^{-1}_{M_2,L_2} \end{bmatrix}, \text{ and } \mathbf{R}' = \begin{bmatrix} R_{-M_1,-L_1} \\ R_{(M_1+1),-L_1} \\ \cdot \\ \cdot \\ R_{-M_2,-L_1} \\ R_{-M_1,-(L_1+1)} \\ \cdot \\ \cdot \\ R_{-M_1,-L_2} \\ \cdot \\ \cdot \\ R_{-M_2,-L_2} \end{bmatrix}. \tag{13}$$

The elements of the above vectors are

$$(\underline{\bar{\mathbf{R}}}'^{-1})_\mu = \bar{R}^{-1}_{i,j},$$

and

$$(\mathbf{R}')_\nu = R_{-k,-\ell},$$

where

$$j = int\left[\frac{(\mu-1)}{(M_2-M_1+1)}\right] + L_1,$$

$$\ell = int\left[\frac{(\nu-1)}{(M_2-M_1+1)}\right] + L_1,$$

$$i = \mu - 1 - (j-L_1)\cdot(M_2-M_1+1) + M_1,$$

$$k = \nu - 1 - (\ell-L_1)\cdot(M_2-M_1+1) + M_1. \tag{14}$$

We can now write equation (11) as:

$$\sum_{\mu=1}^{(M_2-M_1+1)\cdot(L_2-L_1+1)} (\underline{\bar{\mathbf{R}}}'^{-1})_\mu \cdot (\underline{\mathbf{A}}')_{\mu\nu} = (\mathbf{R}')_\nu,$$

$$\nu = 1, \ldots, (M_2-M_1+1)\cdot(L_2-L_1+1),$$

or

$$\underline{\bar{\mathbf{R}}}'^{-1} \cdot \underline{\mathbf{A}}' = \mathbf{R}', \tag{15}$$

where $\underline{\mathbf{A}}'$ is a $[(M_2-M_1+1)\cdot(L_2-L_1+1)]^2$ matrix and

$$(\underline{\mathbf{A}}')_{\mu\nu} = A_{k-i,\ell-j}.$$

Using equations (14) we can easily see that $\underline{\mathbf{A}}'$ is a symmetric matrix since:

$$(\underline{\mathbf{A}}')_{\mu\nu} = A_{k-i,\ell-j}$$

and

$$(\underline{\mathbf{A}}')_{\nu\mu} = A_{i-k,j-\ell} = A_{-(k-i),-(\ell-j)} = A_{k-i,\ell-j},$$

since we know that the autocorrelation function $A_{\alpha,\beta} = A_{-\alpha,-\beta}$. Therefore

$$(\underline{\mathbf{A}}')_{\mu\nu} = (\underline{\mathbf{A}}')_{\nu\mu}.$$

Because $\underline{\mathbf{A}}'$ is a symmetric matrix, equation (15) can be solved very quickly by Levinson's method for Toeplitz matrices.

Employing equation (15) several filters were produced. Two of them have been tabulated in Table 1; these are denoted as F2 and F2A, respectively. The parameters of the model used to produce the respective filters are also given in the Table. These filters were selected for demonstration purposes. The difference between the filter F2 and F2A is that the latter consists of 7×7 elements as compared to 5×5 elements for the first. In both cases, the model was a cube with 1 m sides.

Figures 3 and 4 show the 2-D convolution of filters F2 and F2A with the respective shape functions that were inverted to produce these filters. As was expected, the filter F2A, which is longer in both directions than F2, performs better, giving a result that is less noisy and more sharp. The sharpness of the response of F2A comes closer to the shape of the actual surface projection of the disturbing body.

APPLICATION OF SYNTHETIC DATA

To check the performance and applicability of the filters, two artificially constructed data sets were employed. In both cases, we used models that simulate structures that often occur in the archaeological search. The total magnetic field effect was calculated using the algorithm given by Bhattacharyya (1964) for all the synthetic examples presented in these pages.

Figure 5 shows the result after convolution of filter F2 with the anomaly produced by a thin rectangular slab buried at 1 m depth. The slab is positively magnetized with respect to the environment, with a susceptibility contrast of 0.0005. It has a depth extent of 1 m and a cross section of 5×5 m^2.

The result of convolution of F2 with the total field anomaly produced by a model that represents the ruins of the foundation of a building are shown in Figure 6. The ruins are supposed to be composed of walls of 5 m length and 1 m width buried at a 1 m depth. The susceptibility contrast is -0.0005.

The influence of variation of the burial depth is illustrated in Figure 7. The filter F2A was convolved with the response of a prism. The prism, buried at various depths, has the same dimensions as the one used to calculate the filter. The different depths are 0.5, 2, and 3 grid units. The models in plan view, along with the resulting magnetic total field anomaly, are shown in parts a, b, and c of Figure 7. The

corresponding distributions of shape functions are shown in Figure 7d, e, and f. As we progress in burial depth, broadening of the resulting pattern along with magnitude reduction are observed. This is expected because we are essentially dealing with upward continuation of the total field anomalies.

The lateral resolving ability of the filtering procedure is demonstrated in Figure 8. Two identical prisms are shown in Figure 8a, buried at 1 grid unit depth with their centers at a spacing of 2 grid units, along with their total field anomaly. In Figure 8b, the same prisms are translated such that their centers are at 2.5 grid units apart. In Figure 8c, the susceptibility contrast of the right-hand prism is reversed to -0.0005, and the distance between the prism centers is kept at 2.5 grid units. In all other cases, the susceptibility contrast is 0.0005. When the prism centers are 2.5 grid units apart, the distribution of the shape function shows two distinct peaks (Figure 8e and f). Again, this effect was expected since the Nyquist wavenumber in the present cases is 0.5 (grid units)$^{-1}$. Although the distinction of the two peaks is obvious in Figure 8e, it can be justified using the Rayleigh criterion as well. In our case, this criterion is stated as the inequality

$$J_T < \frac{8}{\pi_2} J_P, \tag{16}$$

where J_T and J_P are the magnitudes of the amplitude function (magnetization) at the trough between the peaks and the peaks themselves, respectively. In Figure 8d, the Rayleigh inequality is fulfilled. This is the less pronounced case where the body centers are located one Nyquist wavelength apart; namely, the peak value is 1.18 and the trough 0.83.

APPLICATION TO DATA FROM ARCHAEOLOGICAL EXPLORATION

Figure 9 shows the total magnetic field map over a location near the defensive wall of the ancient city of Aegae (Verghina) in Northern Greece. The visible part of the remains of the defensive wall has been drawn in the same figure. The object of the exploration was to trace the wall and locate other features that could possibly be concealed beside the wall.

The antiquities are in an environment of highly magnetic drift material. The data was collected using a proton-precession magnetometer at traverses 1 m apart and at 1 m intervals along each transverse. Another magnetometer of the same type served as a base station to correct the values for the daily variation of the earth's magnetic field.

The masonry material commonly used in this area consists of hewn stone blocks of Diabase (Dolerite), which again is a highly magnetic ultrabasic rock. The less common material is limestone blocks which have negligible magnetic susceptibility.

Attempting a qualitative interpretation of the total field map we can say that the response of the defensive wall can hardly be identified. A broader linear feature strikes in the same direction as the wall, while several other anomalies that obscure the whole situation appear on the map.

The distribution of the amplitude function, after application of the F2 filter to the total field data, is presented in Figure 10. Two trial trenches were dug in the explored locations and are marked as A and B in Figure 10. Nothing was found in trench A, while the relics of the wall and the foundations of a tower were revealed in trench B. Apparent susceptibility measurements conducted on samples of the

Table 1. Parameters used for the evaluation of the F2 and F2A filters and the resulting numerical values.

	Parameters of the Model						
	Inclination of the earth's total field: 54°						
	Declination of the earth's total field with respect to y-axis: 90°						
	Burial depth (depth to the top of the prism): 1 m						
	Depth extend: 1 m						
	Thickness along north-south direction (x-axis): 1 m						
	Half strike length (y-axis): 0.5 m						
	Dip of the prism: 90°						
	Number of thin plates used to generate the prism: 11						
	Filter Coefficients						
	Filter F2						
	0.002	0.006	0.01	0.006	0.002		
	−0.01	−0.005	0.05	0.005	−0.01		
↑	0.06	−0.29	0.64	−0.29	0.06		
N	−0.03	0.16	−0.47	0.16	−0.03		
	0.007	−0.06	0.2	−0.06	0.007		
	Filter F2A						
	0	0.001	0.006	0.011	0.006	0.001	0
	−0.001	−0.001	−0.003	0.002	−0.003	−0.001	−0.001
	−0.0002	−0.0025	0.006	0.025	0.006	−0.0025	−0.0002
	−0.01	0.041	−0.17	0.38	−0.17	0.041	−0.01
↑	0.0003	−0.014	0.089	−0.298	0.089	−0.014	0.0003
N	0.0001	0.0024	−0.043	0.166	−0.043	0.0024	0.0001
	−0.0016	−0.0005	0.0156	−0.0709	0.0156	−0.0005	−0.0016

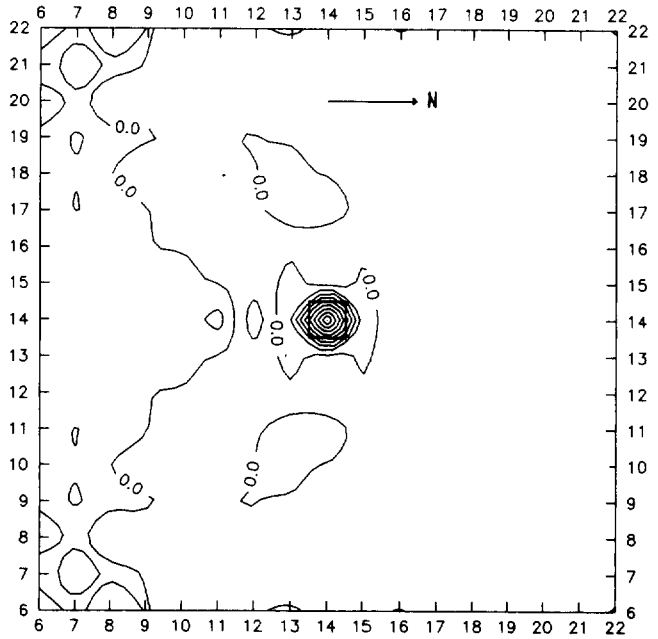

FIG. 3. Contour map of the result of the convolution of filter F2 with the respective shape function of the model used to evaluate the filter.

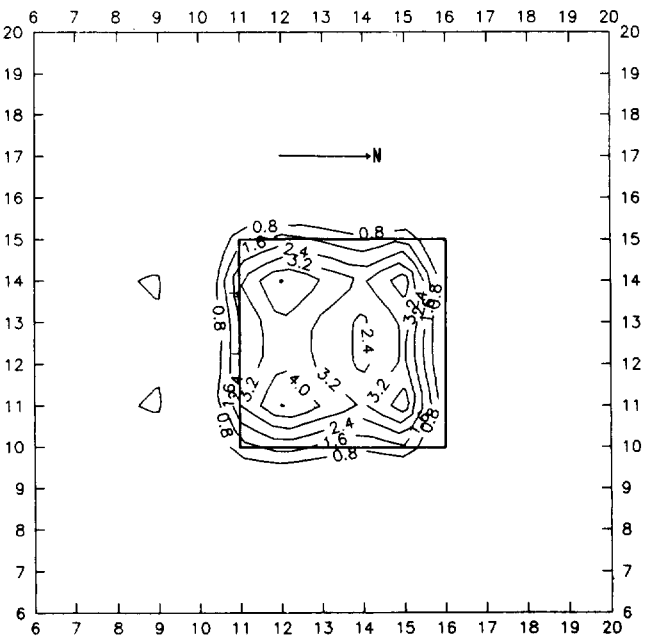

FIG. 5. The result of convolution of filter F2 with a total magnetic field anomaly produced using a horizontal thin slab model. The plan view of the model is shown as the solid line.

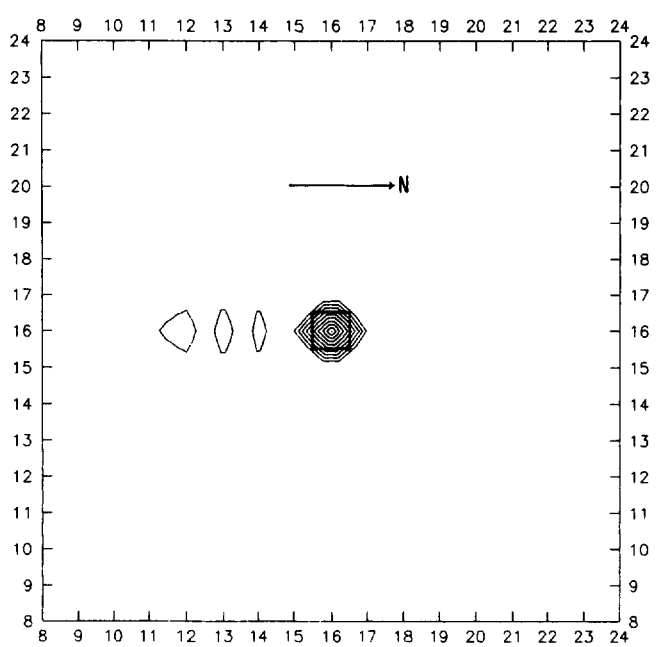

FIG. 4. Contour map of the result of the convolution of filter F2A with the respective shape function of the model used to evaluate the filter.

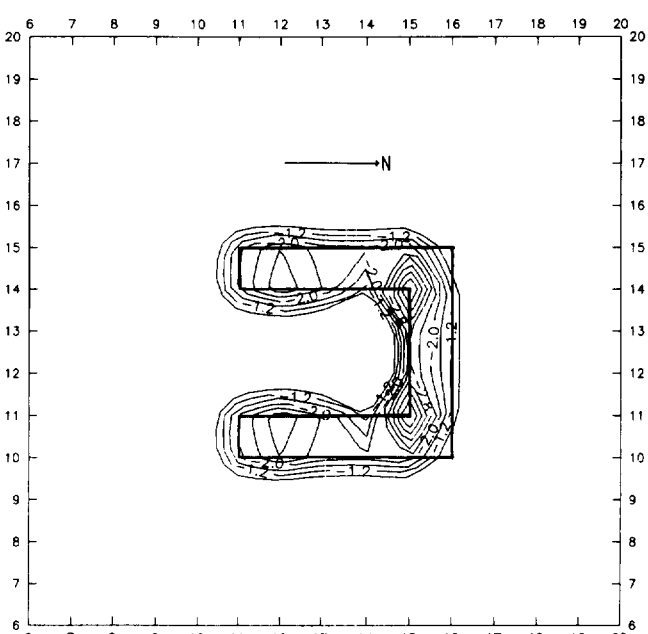

FIG. 6. The result of convolution of filter F2 with the calculated total magnetic field anomaly using the model whose plan view is shown by the solid line.

revealed features are shown in Table 2. It is evident, that the doleritic blocks and the infilling of the initial construction ditch are responsible for the anomalies in Figure 10.

DISCUSSION

With respect to the examples presented, both synthetic and actual, it is obvious that the proposed procedure achieves its best performance if the positive and negative values are plotted separately. This is a compromise to avoid any confusion that might be created if an attempt is made to interpret the initial amplitude function distribution maps. Alternatively, we could hatch the areas of positive values on a single map, or present the result as a dot-density image, but in any case of presentation, the common feature is that the inversion filters function in a manner similar to a reduction to the pole.

A crucial point of the whole procedure is the selection of burial depth for the models used to produce the filters. In the example presented of ancient Aegae, the burial depth was known to be about 0.5 m below the ground surface, and the magnetometer sensor was fixed at 0.5 m above the surface. Hence, the overall burial depth was 1 m. An estimate of depth level where the antiquities are expected is necessary and is easily accomplished if a trial pit exists at the site under study. Alternatively, historical-archaeological or any other sort of information about the site can be used.

The question of the appropriate filter length has been posed in Tsokas et al. (1991) who constructed 1-D filters in an attempt to modify the original procedure of Karousova and Karous (1989). The optimum length is the distance at which the autocorrelation of the shape function (input wavelet) vanishes. This is the choice generally used in reflection seismology (Yilmaz, 1986). However, such a consideration in the present case will result in large filters that are inconvenient.

The separation of the total field anomaly into amplitude and shape-controlling factors can be seen as a formulation of the susceptibility mapping procedure. The recovered amplitude function distribution is by definition [equation (4)] the spatial distribution of the magnetization vector magnitude. A simple division by the normal field magnitude would yield a rough estimate of the distribution of the susceptibility con-

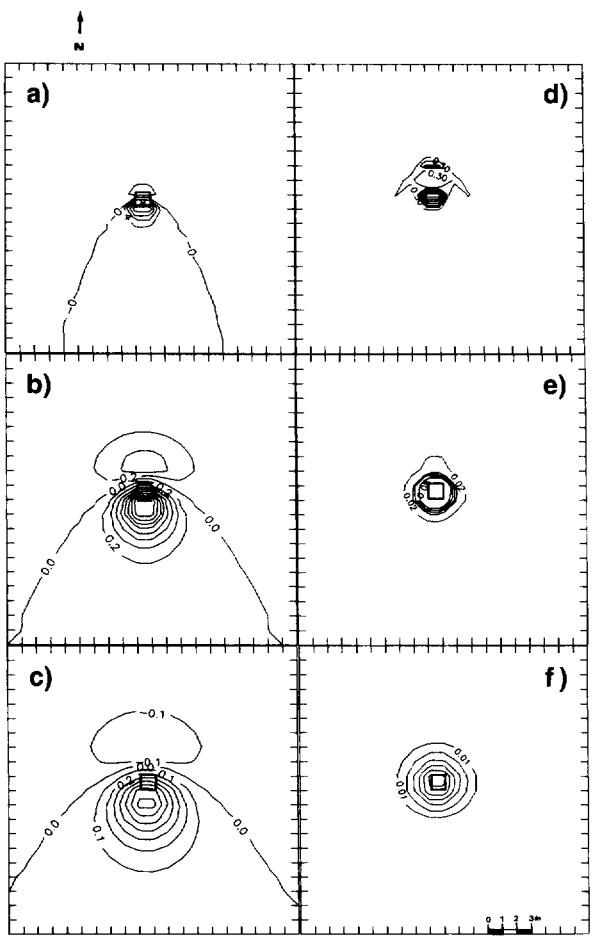

FIG. 7. Presentation of the effect of varying burial depth. The cross-section of a vertical-sided prism is shown as a solid line. The dimensions of the prism are all 1 m and its susceptibility contrast is +0.0005. The computed effects for burial depths of 0.5, 2, and 3 m are shown in (a), (b), and (c), respectively. The resulting distribution of strength functions is shown correspondingly in (d), (e), and (f).

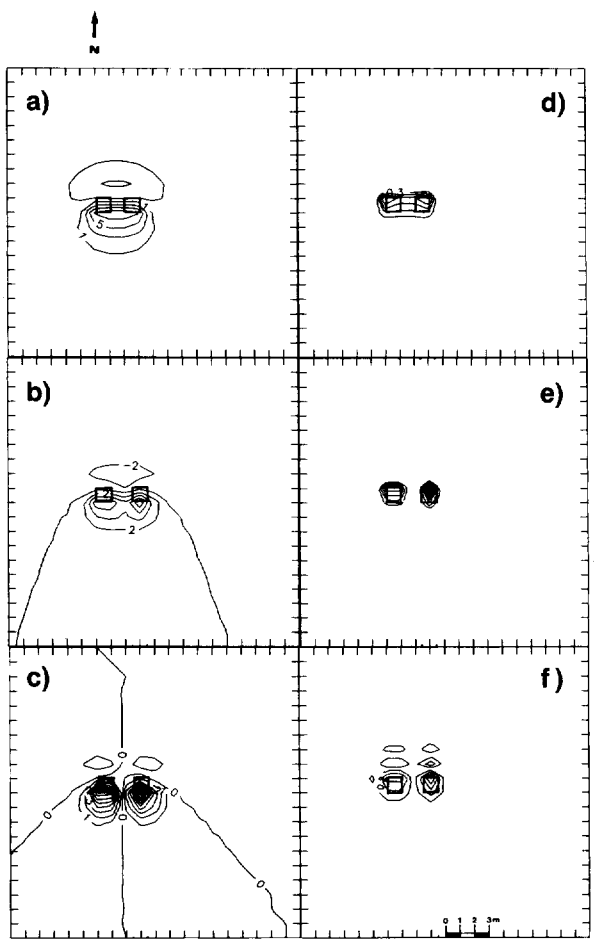

FIG. 8. Presentation of the resolving ability of the proposed procedure. Two identical prisms having all their dimensions 1 m and buried at 1 m depth are shown. Their centers are located 1 m apart in (a) and 2.5 m apart in (b) and (c). The right-hand side prism of (c) is the only one with a negative susceptibility contrast of −0.0005. The results after application of filter F2A are shown in (d), (e), and (f), correspondingly.

trast. Therefore, the proposed filtering can be used to acquire a rough estimate of the susceptibilty contrast.

Susceptibility mapping is usually performed as a frequency domain operation which is based on Bhattarchayya's (1966) expressions for the spectrum of the magnetic field. The space-domain procedure presented here is particularly advantageous if the survey area is small or if the case is 1-D, because convolution involving a short array such as a filter operator is relatively faster than doing Fourier transforms (Yilmaz, 1986). In the 1-D case, even a hand calculator is adequate for the job (Tsokas et al., 1991). However, the method was developed to transform magnetic data from archaeological explorations in an image form that should look much like the excavation result, i.e., the plan view of the ruins.Therefore, the method was designed to rectify the magnetic anomalies and present the maxima and minima of the transformed values directly above the centers of the disturbing bodies. These goals were satisfactorily approached. Also, the lateral extent of the disturbing bodies is fairly well delineated as demonstrated by the synthetic examples.

In general, the use of the proposed filtering procedure is not necessarily confined to archaeological exploration only. It can also be used in ore prospecting, especially where the structures appear repetitive. The model of the thin magnetic sheet can easily be built up from the McGrath and Hood formula.

Finally, the superposition principle was involved twice in the filter's evaluation and was presumed to hold true. This is self evident in cases of archaeological search when magnetization is, in general, of low magntiude. Certainly it is not the case when the magnetization is strong.

CONCLUSIONS

The proposed procedure for construction of inverse filters and their convolution with the total magnetic field data seems to function satisfactorily in archaelogical geophysics. The results are maps of the spatial distribution of the amplitude function, which by definition coincide with the magnitude of the magnetization vector. The anomalies on the resulting maps are located directly over the disturbing structures. The spatial extent of the structures is approximately given by the extent of the anomalies.

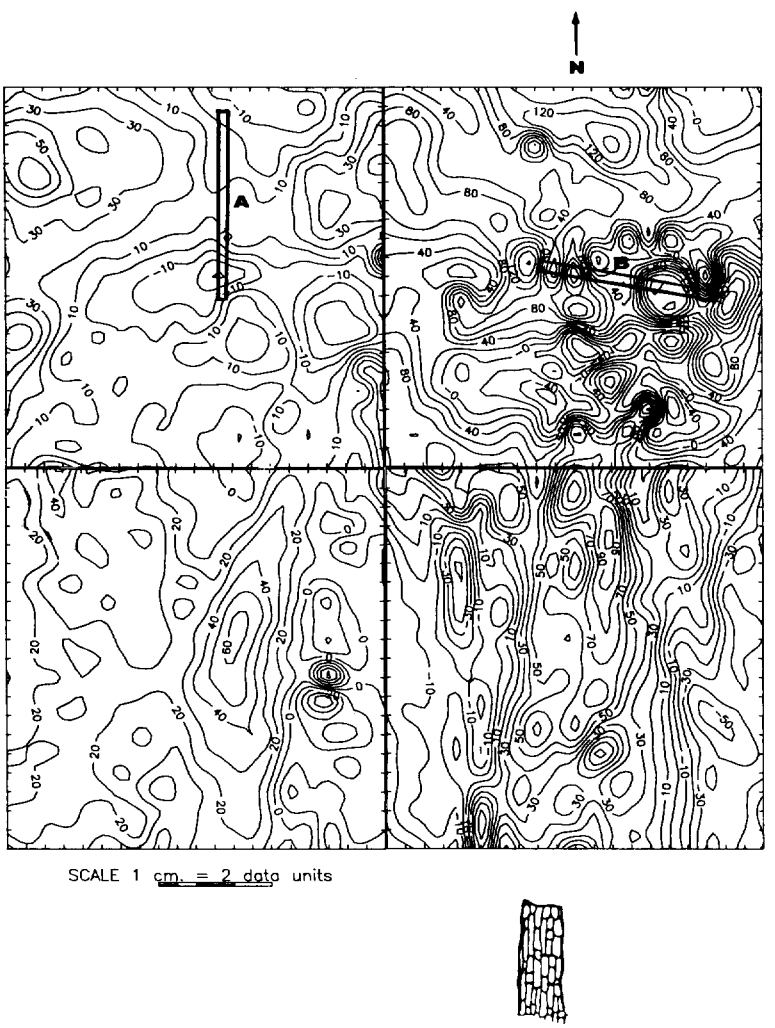

FIG. 9. Distribution of the total magnetic field in an area 40 × 40 m^2 at the archaeological site of Aegaes (N. Greece). The visible ruins of a defensive wall are also drawn in the figure. The survey was conducted on four subgrids with an area 20 × 20 m^2.

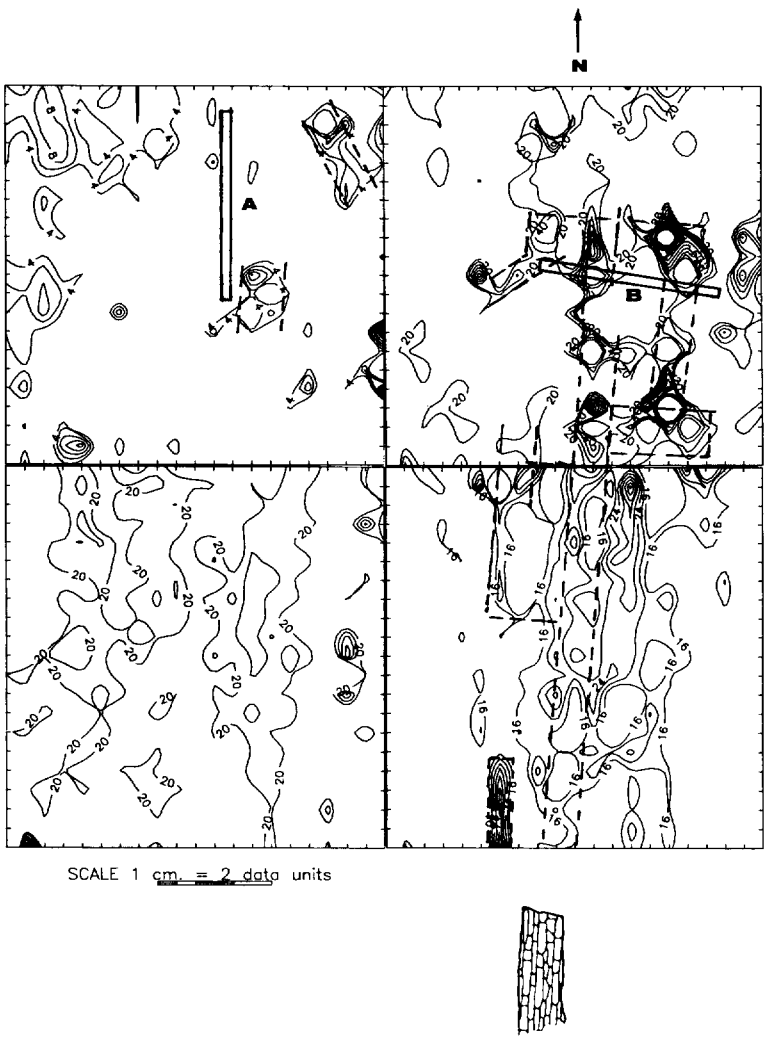

FIG. 10. Distribution of the strength function resulting after convolution of filter F2 with the data of Figure 9. Filtering was performed separately on each subgrid. The suggested wall course, as delineated by the strength function anomaly, is marked with a dashed line. Anomalies attributed to other relics, including the ruins of a defensive tower, are also marked with dashed lines. The broader linear anomaly on which the effect of the defensive wall is superimposed was attributed to the ditch opened for the construction of the wall. The interpretation was confirmed by the findings of the trial trenches A and B which were dug after the geophysical exploration of the site.

Table 2. Apparent susceptibility measurements conducted on the findings of the trial trenches.

	Feature	Number of Samples	Mean Value of Apparent Susceptibility
TRENCE A	1. Topsoil	13	33.1×10^{-4}
	2. Subsoil	6	55.5×10^{-5}
TRENCE B	1. Topsoil	15	31.5×10^{-4}
	2. Subsoil*	9	10.7×10^{-3}
	3. Doleritic blocks	6	26.3×10^{-3}

* At the location of the ancient ditch (dug for the foundation of the wall)

The results can be considered as an approximate image of the plan view of the relics. This fact contributes to the rapid location and identification of excavation targets.

REFERENCES

Bhattacharyya, B. K., 1964, Magnetic anomalies due to prism-shaped bodies with arbitrary polarization: Geophysics, **29**, 517–531.

——— 1966, Continuous spectrum of the total magnetic field anomaly due to a rectangular prismatic body: Geophysics, **31**, 97–121.

Bhattacharyya, B. K., and Chan, K. C., 1977, Computation of gravity and magnetic anomalies due to inhomogeneous distribution of magnetization and density in a localized region: Geophysics, **42**, 602–609.

Bhattacharyya, B. K., and Navolio, M. D., 1975, Digital convolution for computing gravity and magnetic anomalies due to arbitrary bodies: Geophysics, **40**, 981–992.

Grant, F. S., and West, G. F., 1965, Interpretation theory in applied geophysics: McGraw-Hill Book Co.

Kanasewitch, E. R., 1975, Time sequence analysis in geophysics. Univ. of Alberta press.

Karousova, O., and Karous, M., 1989, Deconvolution of ΔT profile curves: Presented at the Internat. Symp. on computer applications and quantitative methods in archaeology: Univ. of York and York Archaeological Authorities, U.K.

McGrath, P. H., and Hood, P. J., 1973, An automatic least-squares multimodel method for magnetic interpretation: Geophysics, **38**, 349–358.

Scollar, I., Weidner, B., and Segeth, K., 1986, Display of archaeological magnetic data: Geophysics, **51**, 623–633.

Tsokas, G. N., Papazachos, C. B., Loucoyiannakis, M. Z., and Karousova, O., 1991, Inversion filters for the transformation of geophysical data from archaeological sites based on the vertical-sided finite prism model: Archaeometry, **33**, 215–230.

Wynn, J. C., 1986, Archaeologial prospection: An introduction to the special issue: Geophysics, **51**, 533–537.

Yilmaz, O., 1986, Seismic data processing: Elsevier Science Publ. Co., Inc.